Title
APPLICATION OF SPHERICAL GRATINGS IN SYNCHROTRON RADIATION SPECTROSCOPY

Authors
Hogrefe, H.
Howells, M.R.
Hoyer, E.

Publication Date
1986-05-01

Lawrence Berkeley Laboratory
UNIVERSITY OF CALIFORNIA

Accelerator & Fusion Research Division

Center for X-Ray Optics

Presented at the International Conference on
Soft X-Ray Optics and Technology,
Berlin, FRG, December 8-11, 1986

APPLICATION OF SPHERICAL GRATINGS IN SYNCHROTRON RADIATION SPECTROSCOPY

H. Hogrefe, M.R. Howells, and E. Hoyer

May 1986

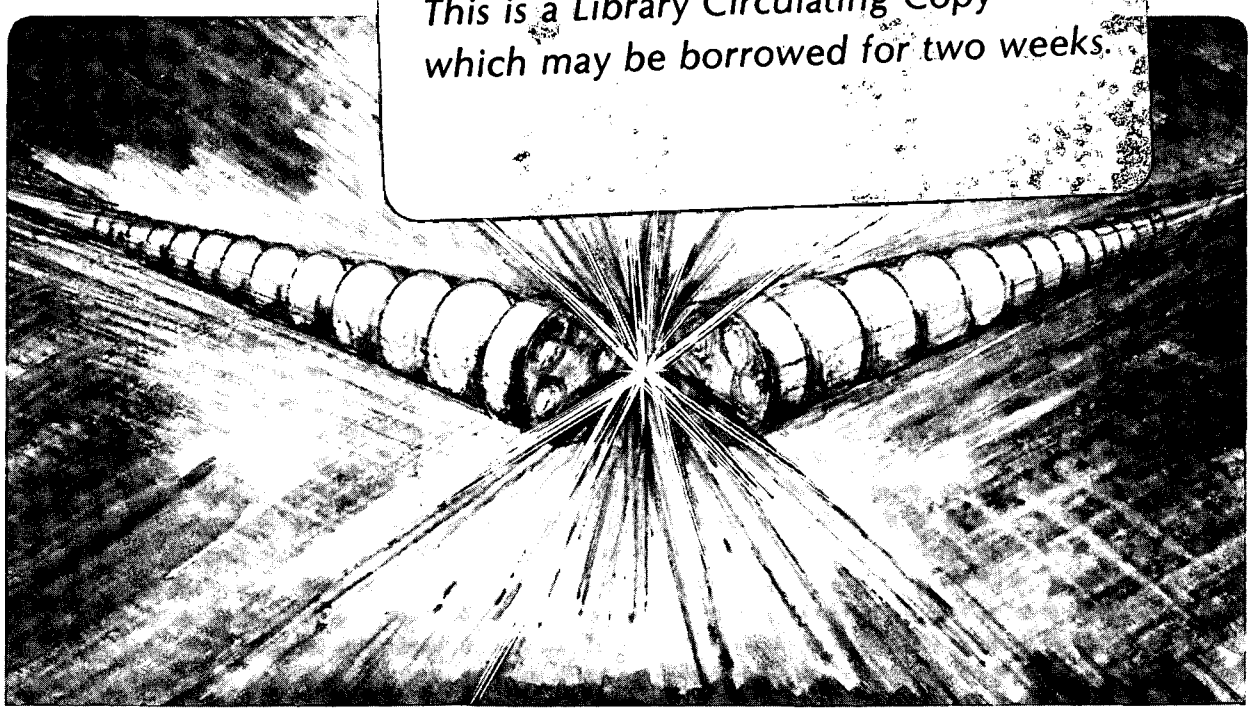

Prepared for the U.S. Department of Energy under Contract DE-AC03-76SF00098

DISCLAIMER

LBL-22070

Application of Spherical Gratings in Synchrotron Radiation Spectroscopy

H. Hogrefe, M.R. Howells, and E. Hoyer

Center for X-Ray Optics
Lawrence Berkeley Laboratory
University of California
Berkeley, California 94720

December 1986

Application of Spherical Gratings in Synchrotron Radiation Spectroscopy

H. Hogrefe, M.R. Howells and E. Hoyer

Center for X-Ray Optics, Lawrence Berkeley Laboratory
Berkeley, CA 94720, USA

Abstract

The recent development in grazing incidence grating monochromator design is discussed and the performance limiting factors for such instruments are examined. Especially the aberrations of toroidal and spherical gratings are investigated using the optical path function concept. It is shown that large radius spherical gratings, which can be produced with better slope tolerances than aspherics, also yield smaller overall line curvature than toroids. Therefore, a new simple spherical grating monochromator design is proposed and its performance is analyzed.

Introduction

For some time now synchrotron radiation emitted by relativistic electrons in synchrotrons and storage rings has been utilized as a radiation source for various scientific investigations. The spectral region where this type of light source is attractive is mainly from the near ultra-violet starting at about 3000Å down to around the molybdenum K_α line at 0.7Å. Applications outside this region exist but are less popular. The region breaks down into fairly distinct sections according to the type of technology that must be used in spectroscopic instruments. The spectral content of synchrotron radiation is normally white and if spectral peaks exist they are not generally narrow enough to use. Consequently it is almost always necessary to use a monochromator. The design of monochromators for use with synchrotron radiation has received considerable attention and a number of reviews exist. The one by Johnson [1] is the most complete. We list in Table I the general classes of monochromator which are of interest for synchrotron radiation applications.

Table 1

Synchrotron radiation monochromator types

	Wavelength range (Å)	Critical angle for Au (°)	Dispersive element	Comments
1.	0.7 - 4.0	.25 - 1.3	crystals	good technology
2.	4.0 - 12.0	1.3 - 3.5	special crystals or grazing incidence gratings	most difficult region
3.	12.0 - 300	3.5 - 37	grazing incidence gratings	difficult region
4.	300 - 3000	NA	normal incidence gratings	good technology

Historically regions 1 and 4 have been well served with instruments having good resolution and phase space acceptance. In other words with a good value of the resolving power, phase space acceptance product. The latter quantity forms the best single figure of merit for these systems. Region 2 is defined roughly as the region where gratings are inefficient and difficult and beryllium windows strong enough to withstand atmospheric pressure cannot be used. The problems of working with crystals with large inter-planar spacing adds to the difficulties of working in this region and the overall effect is that relatively little work has been done in region 2 using synchrotron radiation with a monochromator. In region 3, gratings work with good efficiency but the use of grazing angles reduces the phase space acceptance and good quality focusing and collimating optics are hard to find. The result has been in the past that monochromators in region 3 have had poor resolution and low phase space acceptance. It is the purpose of this article to discuss the limitations of monochromators in this spectral region and to reach an understanding which can form the basis of the design of a new generation of monochromators which achieve substantial improvement in both the resolution and phase space acceptance compared to earlier designs.

Resolution limits

The best resolution values published so far, for grazing incidence grating monochromators using synchrotron radiation are those of Petersen [2] and Himpsel [3]. These workers quote values of about 0.2 eV at the carbon edge, or a resolving power of about 1400. Eberhardt has recently obtained somewhat better values: 0.1 eV at the nitrogen edge, or a resolving power of about 4000 [4]. In all these cases an extraordinary sacrifice of flux was required in order to obtain the best resolution. For Petersen, using the SX700 plane grating monochromator, including one ellipsoidal mirror, it was necessary to restrict the system to only 3% of full aperture to find a portion of the optical surfaces accurate enough to give the image quality required for 0.2 eV resolution. For Himpsel, working with a toroidal grating monochromator, the issue was probably aberrations and again these could be controlled only by a substantial reduction in aperture. In the case of Eberhardt using a GRASSHOPPER (5 m spherical grating) monochromator, the resolution limit was probably the slit width which would need to be 5 μm for the 1200 ℓ/mm grating employed.

These three cases illustrate nicely the three main types of resolution limitation which are important for this type of monochromator. These are:

(i) Optical fabrication tolerances which are especially important for systems containing aspheric surfaces.
(ii) Aberrations which are worst for toroids on account of the steep sagittal curvature of these surfaces.
(iii) Slit width which is usually most important for spherical gratings.

In the past the characteristics of the synchrotron radiation source, namely the emittance, have also been a limiting factor but this will be improved with modern storage ring designs. In the future we expect that thermal distortion will become important and we have already begun to address that. For the time being we consider the three issues mentioned above in more detail.

Optical fabrication tolerances

The art of optical fabrication has progressed considerably over the centuries and one can now obtain surfaces of more or less any shape and size at a price. The X-ray astronomy community have devoted great efforts to designing and fabricating large exotic shaped surfaces such as the Wolter-Schwarzschild double bounce telescope system. Special polishing systems and measurement instrumentation are constructed and low scatter surfaces with tolerances in the arc second region can be made. For example the 0.7 m long Einstein telescope had 50% encircled energy within 2 arc second of theoretical, a surface roughness of 14-25 Å rms (measured by visible light scattering) and a price tag of $4 million [5]. This represented early 1970's optical technology.

The current state-of-the-art in this area is represented by the so-called "Technology mirror assembly" built by Perkin Elmer for the Advanced X-ray Astronomical Facility (AXAF). This telescope, which is of comparable size to the Einstein, achieved an image width of 0.38 arc seconds for a point source at large distance [6]. This spread includes the manufacturing tolerances of both reflecting surfaces and the process of assembling them together. There is no doubt that even better tolerances than this can be achieved for the much simpler optics required for synchrotron radiation applications. In fact, a primary theme of this paper is to make the case that spherical surfaces are attractive for high resolution systems for just this reason. We believe that spherical surfaces of the required quality have been available for many years as we will shortly demonstrate.

For synchrotron radiation applications it is necessary to use fabrication methods and design choices that allow larger numbers of optics to be fabricated at reasonable prices. For optics which have a suitable axis of symmetry (i.e. conics of revolution but not toroids), single point diamond machining provides a convenient way to manufacture considerable numbers of optics of any shape with good surface slope tolerances. However, in order to achieve a low scatter finish the surfaces must be subjected to a polishing process which can be made to maintain the initially good surface figure only if a suitable method of surface measurement is available. Other methods of fabricating aspheric surfaces similarly end with polishing stages, and it is the lack of generally available measurement instrumentation that prevents all these techniques from achieving the tolerances needed for building a high resolution soft X-ray monochromator. The exceptions to this are spherical and flat optics. There have long been techniques by which good craftsmen could make and measure spherical and flat optics with sub arc second tolerances. For example many first class optics have been made using the Foucault test. In recent times it has become possible to measure flat and spherical optics over the entire range of spatial wavelengths of interest here (about 10 μm - 0.1 m) using commercially available measuring equipment [7] that provides a permanent record to document the surface quality.

In evaluating resolution values limited by both fabrication tolerances and slit widths we can use the basic equation for the slit width limited resolution $\Delta\lambda_S$ for a grating with the groove spacing d:

$$\Delta\lambda_S = \frac{\cos\alpha\ s d}{r} = \frac{\cos\beta\ s' d}{r'} \qquad (1)$$

where s is the entrance slit width, s' the width of its image, α and β are the angle of incidence and diffraction respectively, r and r' are as shown in Figure 1.

Anticipating the monochromator design that we describe later in this paper and assuming that 10μm slits are the smallest practical size, we arrive at a value of 0.5μrad for the allowed r.m.s. slope error. This is 1.2 μrad full width half maximum for the spread function of slope errors. This is a challenging tolerance which needs to be defined and specified as a combination of a geometrical optical slope tolerance over the full aperture and a wave optical tolerance over a subaperture [8]. These are both in addition to the usual finish specification. We do not wish to discuss the determination of tolerances in detail here. However, we must note that the quoted tolerances on the best aspheric surfaces are usually in the range 5 - 10 arc seconds, and for spherical or flat surfaces around one arc second. The latter figure really represents a limitation of measurement technique rather than fabrication ability, but even with that reservation we see that for resolution determining optics, spherical surfaces have a great advantage. As a further verification of this we can consider the demonstrated resolution capabilities of spherical gratings in the normal incidence regime. For example Ito et al. [9] recently reported a resolving power of > 2.5 x 10^5 at λ = 790Å in the 7^{th} order of an off-the-shelf replica grating [10] of 6.65 m radius and 1200 ℓ/mm. According to equation (1) this implies an s/r value of 2.7 μradian. We may thus estimate an upper limit for the slope error of the grating surface as about 0.7 μradian. Even higher spectral resolution was demonstrated in the classical experiments of Hertzberg in the 1950's. The Lamb shifts in the n = 1 levels of various atomic species [11] were measured with accuracies which translate to surface slope tolerances of less then one microradian in the 3m radius spherical grating that was used.

This type of information is actually more meaningful from a spectroscopy point of view than optical shop measurements. The best way to circumvent the optical fabrication tolerance problem would appear to be to use a replica grating off the same master as one that had been proved in the above way. Even if this is not possible, spherical surfaces are clearly the optic of choice for high resolution applications.

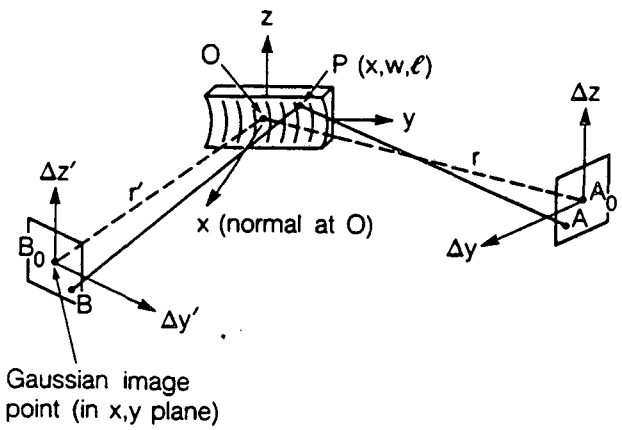

Figure 1. Notation for grating aberration analysis.

Aberrations

In order to discuss the influence of aberrations, we utilize the analysis of the imaging performance of a grating in terms of the optical path function. We specialize to the case of a toroidal surface (of which the spherical is a special case) and we consider only the conventional in-plane applications of a Rowland grating, i.e., a grating whose grooves are the intersection of the substrate with a set of parallel equispaced planes. Following Noda, Namioka and Seya [12], we write the optical path function expansion to sufficiently good approximation as in equation (2):

$$F = F_{000} + wF_{100} + \ell F_{011} + w\ell F_{111} + \frac{1}{2} wF_{102} + \frac{1}{2} w^2 F_{200}$$

$$+ \frac{1}{2} \ell^2 F_{020} + \frac{1}{2} w\ell^2 F_{120} + \frac{1}{2} w^3 F_{300} + \frac{1}{8} w^4 F_{400} + \ldots w^i \ell^j F_{ijk} (\Delta z^k) + \ldots \qquad (2)$$

where

$$F_{000} = \sum r \qquad \text{Constant term} \qquad (2a)$$

$$F_{100} = \frac{m\lambda}{d} - \sum \sin\alpha \qquad \text{Grating equation} \qquad (2b)$$

$$F_{011} = - \sum \frac{\Delta z}{r} \qquad \text{Magnification} \qquad (2c)$$

$$F_{111} = - \sum \frac{\Delta z \sin\alpha}{r^2} \qquad \text{Line shape} \qquad (2d)$$

$$F_{102} = \sum \frac{\Delta z^2 \sin\alpha}{r^2} \qquad \text{Line shape} \qquad (2e)$$

$$F_{200} = \sum T \qquad \text{Defocus} \qquad (2f)$$

$$F_{020} = \sum S \qquad \text{Astigmatism} \qquad (2g)$$

$$F_{120} = \sum \frac{S \sin\alpha}{r} \qquad \text{Astigmatic coma} \qquad (2h)$$

$$F_{300} = \sum \frac{T \sin\alpha}{r} \qquad \text{Primary coma} \qquad (2i)$$

$$F_{400} = \sum \left(\frac{4 T \sin^2\alpha}{r^2} - \frac{T^2}{r} + \frac{S}{R^2} \right) \qquad \text{Spherical Aberration} \qquad (2j)$$

$$\text{with } T = \frac{\cos^2\alpha}{r} - \frac{\cos\alpha}{R}, \quad S = \frac{1}{r} - \frac{\cos\alpha}{\rho}$$

where R and ρ are the major and minor radii of the toroid respectively. The other notation is given in Figure 1. The meaning of $\sum$ is that a second term must be added which is identical to the first apart from the replacements $\alpha \to \beta$, $r \to r'$, $\Delta z \to \Delta z'$. We differ slightly from the treatment of Noda et al. by expanding the square roots in their grating equation and magnification terms in order to separate the parts representing line shape. In order to apply the general theory provided by Noda et al. we utilize the following approximation to the toroidal surface

$$x(w,\ell) = \frac{w^2}{2R} + \frac{\ell^2}{2\rho} + \frac{\ell^2 w^2}{4R^2\rho} + \frac{w^4}{8R^3} + \frac{\ell^4}{8\rho^3} + \ldots \qquad (3)$$

For a good focus, it is necessary to satisfy Fermats Principle $(\partial F/\partial \ell) = (\partial F/\partial w) = 0$ as closely as possible. This enables us to obtain the grating equation from the linear term F_{100}

$$m\lambda = d(\sin\alpha + \sin\beta) \qquad (4)$$

For a stigmatic focus we would need to have $F_{200} = F_{020} = 0$ as well and this can indeed be achieved using a toroidal grating.

For a perfect focus we would need to have all the F_{ijk}'s zero which cannot be achieved with a toroid. Non-zero values for the F_{ijk}'s represent particular geometrical optical aberrations as indicated in equation (2) and lead to displacements of

the rays arriving in the image plane from the ideal Gaussian image point. It can be shown that the ray displacements are given by

$$\Delta y'_{ijk} = \frac{r'}{\cos\beta}\frac{\partial F_{ijk}}{\partial w} \qquad \Delta z'_{ijk} = r'\frac{\partial F_{ijk}}{\partial \ell} \tag{5}$$

$$\Delta y' = \sum_{ijk} \Delta y'_{ijk} \qquad \Delta z' = \sum_{ijk} \Delta z'_{ijk}$$

In a simple toroidal grating system with approximately corrected astigmatism illuminated by a point source in the center of the entrance slit, the ray trace might look something like Figure 2 which illustrates the effect of some of the aberrations. We are interested mainly in aberrations in the w, (i.e. $\Delta y'$), direction since they are the ones that affect the resolution. The main ones in Figure 2 are defocus and curvature of the astigmatic focal line. We can eliminate defocus by agreeing to move the monochromator exit slit to the correct focal distance. However, there is no corresponding way that the astigmatic line curvature can be set to zero. We note that the curvature arises from terms in equation (2) that, after differentiation by w, depend on $(\Delta z')^2$. Allowing that astigmatism may not be negligible the line curvature (ℓc) terms are as follows

$$F_{\ell c} = \frac{1}{2}\sum\left(\frac{S\sin\alpha}{r}\right) w\ell^2 + \frac{\sin\beta}{2r'^2}\left(\Delta z'^2 - 2\ell\Delta z'\right)w \tag{6}$$

that is F_{120}. F_{102} and F_{111} with $\Delta z = 0$ (point source illumination). Since $\Delta z = 0$ the value of $\Delta z'$ for any ray is determined only by the astigmatism according to (5) and (2g)

$$\Delta z' = r'\sum(S)\ell \tag{7}$$

Inserting this in (6) and differentiating with respect to w we get

$$\Delta y'_{\ell c} = \frac{\Delta z'^2}{2(\sum(S))^2 r'\cos\beta}\left[\sum\left(\frac{S\sin\alpha}{r}\right) - \frac{2\sin\beta\sum(S)}{r'} + \sin\beta\,(\sum(S))^2\right] \tag{8}$$

which is the general expression for the line curvature for point source illumination: called "astigmatic curvature" in the original work of Beutler [13]. Eq. (8) now displays explicitly the $(\Delta z')^2$ dependance mentioned above. Examination of (8) shows that in the event that astigmatism is negligible, that is $\Delta z' = r'\sum(s)\ell = 0$, then the last two terms in (8) which come from the field variable ($\Delta z'$) dependent terms F_{102} and F_{111} in F, will become zero. The case where this would happen is a toroid whose ρ value was set for exact astigmatism correction at $\rho = \rho_A$ say. The line curvature then comes from the F_{120} term in F only and is typically large and troublesome. The astigmatism correction in a grazing incidence toroid is achieved by the use of steep sagittal curvature (small ρ) and it is intuitively reasonable that such curvature would lead to curvature of the (now very short) astigmatic focal line.

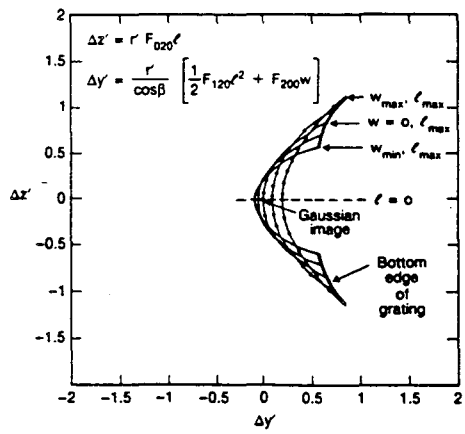

Figure 2. Typical raytrace for a toroidal grating. Defocus F_{200} and astigmatic coma F_{120} are resolution limiting here

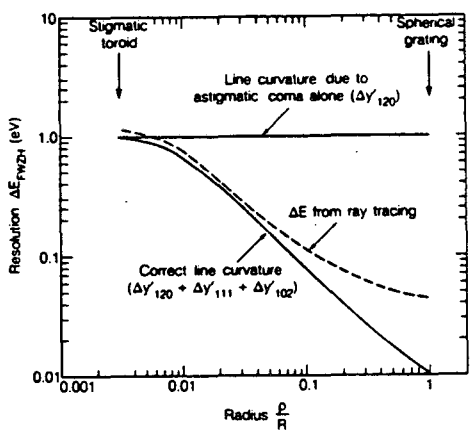

Figure 3. Reduction of line curvature when the sagittal grating radius is enlarged ($\rho \to R$). (Parameters as in Table 2)

In order to remove the astigmatic line curvature we should therefore try increasing ρ. The extreme of this would be to set $\rho = \infty$ i.e., a cylindrical grating. We can see the effect of this by expanding the $\sum$ (S) terms in (8) and eliminating all those terms containing $1/\rho$. For the Rowland circle case, the result for the square bracket term of (8) is:

$$\rho = \rho_A \qquad [\ ] = \frac{\sin\alpha}{r}\left(\frac{1}{r} - \frac{\cos\alpha}{\rho}\right) + \frac{\sin\beta}{r'}\left(\frac{1}{r'} - \frac{\cos\beta}{\rho}\right) \approx \frac{1}{r^2} + \frac{1}{r'^2}$$

$$\rho = \infty \qquad [\ ] = \frac{\sin\alpha + \sin\beta}{r^2} \approx 0$$

Where the $\approx$ sign applies to the case where the approximation $\sin\alpha \approx 1$, $\sin\beta \approx -1$ have been used. We see that a large reduction in line curvature has been achieved. By examining the way the terms cancel or approximately cancel in the expanded form of (8) we can see that in the practical case of a spherical grating ($\rho = R$, $R >> \rho_A$) a similarly large reduction in line curvature is achieved. To show this in a real example we use the proposed monochromator design of a later section and plot in Figure 3 the variation of the energy resolution derived from (8) (that is the spread due to line curvature alone) against ρ as ρ changes from the astigmatism correcting value ρ_A to $\rho = R$. We compare this in the figure with the results of an exact ray trace. We see that the line curvature indeed behaves as expected. It goes from being the dominant aberration accounting for almost all of the line width of the ray trace at $\rho = \rho_A$ to being negligible compared to other aberrations at $\rho = R$. In addition to this good news we get an extra benefit from having ρ large. This is that the acceptance aperture of the grating is now essentially rectangular so it is to be expected that the use of an extended entrance slit would not be harmful. The effect on the focal line in this case is that another kind of line curvature from F_{102} and F_{111} with $\Delta z \neq 0$ is introduced. It is usually called "spectrum line curvature" or by Beutlers name "enveloping curvature". In real cases the two kinds of curvature are combined as explained by Welford [14](see eq. 8). For steeply curved toroids the spectrum line curvature is severe and has a major impact on the resolution. The main point for our purpose however is that with a spherical grating the spectrum line curvature is slight and has only a small effect on resolution.

The conclusion is that long radius spherical gratings do not generate a large overall line curvature and their use solves the problems created by this aberration. This has always been recognized in traditional spectrometer designs which never had line curvature difficulties. The problem has arisen in recent years because the technical ability to make toroids and the attraction of their astigmatism correcting capability has led to a tendency to ignore their disadvantages. The next question is, with no line curvature, which aberration now becomes the limit to resolution? In general the answer is primary coma (F_{300}). However, for Rowland Circle designs ($r = R\cos\alpha$, $r' = R\cos\beta$) F_{300} is identically zero. So assuming we can use a Rowland Circle design we finally become limited by either spherical aberration (F_{400}) or diffraction. The interplay between these two factors has been understood for more than half a century but we do not consider this in detail here [15]. We discuss it in relation to our proposed monochromator design in a later section. Thus we have the overall conclusion that the use of spherical gratings essentially solves the two main problems leading to resolution impairment in present day systems, namely optical fabrication tolerances and aberrations. We now turn to the third.

Slit width limits

In a sense this is not a real limit because all one can expect of a spectrometer is that it achieves its slit width limited resolution. However for a continuum source the throughput of a monochromator diminishes like the square of the width of the slits. (The exit slit width being assumed to be set to match the image of the entrance slit.) Consequently the loss of flux as the slits are closed down for improved resolution is punishing. In addition, there is a limit to how small slits can be made with sufficient perfection and how small the focal spot of a condenser mirror can be. This compromising between flux and resolution reminds us that the goal is to achieve a high resolving power, phase space acceptance product (E). This quantity is often loosely called the "Resolution-luminosity product".

In the plane of dispersion the phase space acceptance (A) of a slit width limited monochromator can be shown to be given by

$$A = N\Delta\lambda_s = \frac{Nds\cos\alpha}{r} \qquad (9)$$

where N is the number of illuminated grooves and we have used equation (1). Obviously E is given by

$$E = N\lambda \tag{10}$$

This is useful but we must first get the resolution we want. In (1) we have quite limited freedom to improve $\Delta\lambda_S$. For systems where the inward and outward ray directions to the grating are fixed the value of d is fixed by spectral range considerations. For a system with an angle 2θ between the inward and outward rays the horizon wavelength $\lambda_H = 2d \cos^2\theta$ in general prevents the use of very dense gratings. However let us rewrite (1) for the Rowland case ($r = R \cos\alpha$)

$$\Delta\lambda_S = \frac{ds}{R} \tag{11}$$

We see that for values of d and s that are limited in the above mentioned ways the only way to improve $\Delta\lambda_S$ is to increase R. This is in fact easy to do for grazing incidence systems. Toroidal grating instruments on synchrotrons already use R values around 50 m which is far higher than is used in traditional Rowland spectrometers. The consequence is that such monochromators are larger than traditional instruments but this is normally quite acceptable. For example for R = 55 m, d = 9091Å and s = 10μm which are reasonable values we get $\Delta\lambda_S = 0.0016$Å which is an attractive value. These parameters are those of the monochromator described in a later section which is ~ 6m long. This is still smaller than many normal incidence instruments which are well established and successful (see for example reference 9). The general conclusion is that it is beneficial to increase the grating radius up to the point where the size of the instrument becomes the enemy of geometrical stability. For soft x-ray undulators on the best modern storage ring sources it is possible to accept the entire beam without loss with 10μm slits using the 55 meter monochromator described later [16].

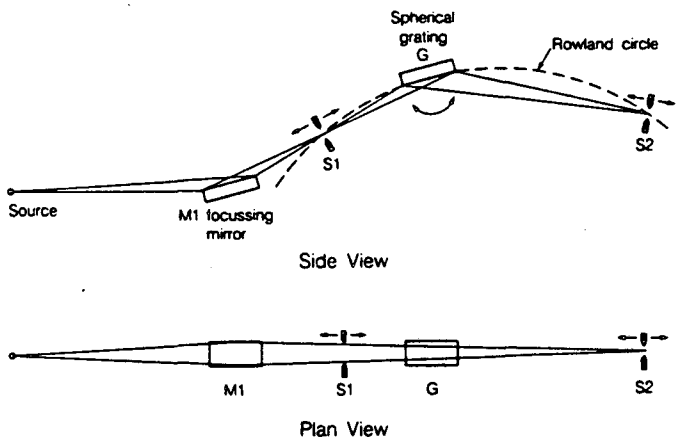

Figure 4. Spherical grating monochromator.

Spherical grating monochromator (SGM)

In the light of the so far described theoretical development one would like to combine the advantages of the spherical grating concepts which provide high spectral resolution with those which offer good light gathering power and simple scan mechanisms. This can be achieved to a considerable degree by the spherical grating monochromator, which will be described in this section and which is based on the spectrograph design of Rense and Violett [17].

Rense and Violett and later also Tondello [18] and Chrisp [19] proposed similar optical instruments mainly for space telescope and plasma spectrograph applications. The most recent application of the same idea is the "High Throughput Monochromator" of Hettrick and Underwood [20]. Rense and Violett were concerned about an optimization of spectral and spatial resolution as well as light gathering power of their devices. For a synchrotron radiation monochromator spatial resolution is not of ultimate importance. Spectral resolution, light gathering power and spectral purity are the important parameters. Moreover, a fixed exit direction is required plus a simple wavelength scan

mechanism compatible with the ultrahigh vacuum environment. For some synchrotron radiation sources, including the SPEAR storage ring at Stanford, the horizontal source size is quite large: 6-8 mm, which is another challenging problem the monochromator design has to take into account. This implies that the entrance slit will be illuminated over a considerable length so that it becomes important to consider any aberrations, for example F_{111} and F_{102} (eq's (2d) and (2e)), that depend on Δz.

Most of the above requirements can be met by the modified Rense and Violett - system shown in Figure 4. The system consists of a toroidal condensing mirror M1 and a spherical grating G, including an entrance slit S1 and exit slit S2 (both moveable along the beam). M1 focuses the synchrotron radiation source in the meridional plane onto the entrance slit S1 of the monochromator. In the sagittal plane M1 makes an image of the source at a distance r_V from M1 behind the grating so that the real sagittal focus is on the exit slit S2 for one wavelength and very near S2 for the whole spectrum. In this way the large astigmatism of the spherical grating at grazing incidence is compensated. Tondello [18] proposed three exchangeable focusing mirrors M1 or a complicated translation of M1 in order to get complete stigmatism also for other wavelengths. This is not necessary in our case since we are not interested in spatial resolution. One could also think of two cylindrical mirrors in Kirkpatrick-Baez configuration as a condensing system instead of the toroid M1 (see e.g. ref. 16). The monochromator itself consists of a large radius spherical grating (straight grooves) and operates on or near the Rowland circle and thereby diminishes the defocus (F_{200}) and coma (F_{300}) aberrations essentially to zero and reduces some fourth order aberrations. As in the case of a standard toroidal grating monochromator (TGM) the diffracted beam is deviated a constant amount from the incoming light: $\alpha - \beta = 2\theta = \text{const.}$ This assures the required fixed exit direction of the monochromatized radiation. The wavelength scan is performed by a simple rotation of the grating. For best resolution the positions of S1 and S2 are adjusted along the line of the principal ray. First of all a convenient wavelength λ_R somewhere in the middle of the scan range of the grating is chosen for which the optical focusing is as shown in Figure 4: M1 focuses on S1 tangentially and S2 sagittally where S1 and S2 have been adjusted along the fixed in and out directions to lie on the Rowland circle for λ_R. The meridional focusing condition is then fulfilled for λ_R

$$F_{200} = \frac{\cos^2\alpha}{r} - \frac{\cos\alpha}{R} + \frac{\cos^2\beta}{r'} - \frac{\cos\beta}{R} = 0$$

and using the Rowland circle solution for the imaging conjugates we have $r=R\cos\alpha$ and $r'=R\cos\beta$. Inserting $r'=R\cos\beta$ into the sagittal focusing condition ($F_{020} = 0$), one can evaluate the imaging conjugate r_s for sagittal focusing and the virtual image distance r_V onto which M1 has to focus, in order to make the image stigmatic for λ_R. Thus we have

$$F_{020} = \frac{1}{r_s} - \frac{\cos\alpha}{R} + \frac{1}{r'} - \frac{\cos\beta}{R} = 0$$

so that

$$r_s = \frac{R}{(\cos\alpha - \sin\beta\tan\beta)} \qquad (12)$$

and

$$r_V = |r_s| + R\cos\alpha + M1S1 \qquad (13)$$

where M1S1 is the distance from the center of the toroid to the slit S1. This gives us all the information needed to calculate the parameters of the condensing toroid in order to compensate the grating astigmatism.

To change the monochromatized wavelength one can either rotate the grating G a certain amount and then (keeping S1 and thereby λ_R fixed) readjust the exit slit S2 for the exact meridional focus, which will then not be on the Rowland circle, or one can rotate G and shift <u>both</u> slits the same amount to again meet the Rowland circle. We shall call the two possibilities mode A and mode B respectively. In mode B the parameter λ_R, which is the wavelength for which the slit positions are set to fulfill the Rowland condition, is changed. From every new λ_R one can cover all output wavelengths λ of that grating with mode A but the aberrations are only minimized when $\lambda = \lambda_R$ holds. Of course mode B is able to provide a better resolution than A but on the other hand this costs some intensity because S1 must be moved out of the meridional focus of the condensing mirror M1. In principal one could fulfill the Rowland circle condition over the whole wavelength range by using scan mode B. In practice we have chosen to compromise somewhat and use mode B for most of the range with some use of mode A at each end. This is because an excessive shifting of slit S1 would cost considerable intensity and would require inconveniently long high precision slides for both slits S1 and S2.

A first realization of the proposed monochromator will be built at the VUV - branchline of beamline VI at the Stanford Synchrotron Radiation Laboratory (SSRL). The actual parameters chosen for this study are based on the requirements of this beamline and are summarized in Table 2. This monochromator will cover the wavelength range from λ=10Å to about 200Å. Using 3 exchangeable gratings of 1100, 500 and 200 lines/mm. Since the optical situation is not changed in principle by changing the line spacing d, we mainly discuss the 1100 ℓ/m grating unless otherwise indicated.

Table 2

Toroidal mirror

Source-mirror distance	16.15 m
Mirror-S1 distance	5.35 m
Meridional Radius R_M	184.3 m
Sagittal radius ρ_M	0.58 m
Angle of incidence	87.5°
Acceptance	1.1 x 1.5 mrad^2 (meridional x sagittal)

Spherical grating

Radius R 55 m			
Deflection angle 2θ		174°	
Grating constant d		1/1100 mm (1/500, 1/200)	
Size		~0.16 x 0.012 m^2	
Slit positions:			
Mode A	λ_R = 20Å	r = 1.72 m	(S1)
		r' = 4.03 - ~4.5 m	(S2)
Mode B	14Å $\leq \lambda_R \leq$ 26Å	r = 2.01 - 1.44 m	(S1)
		r' = 3.68 - ~4.59 m	(S2)

The total length of the beamline is restricted by the available space whereas the minimum distances of M1 and the grating from source are limited by the shield wall of the storage ring SPEAR and the necessity to get enough separation from the hard x-ray branch of beamline VI. Within these limitations we tried make the distance S1-S2, i.e. the grating radius R, as large as possible. Compared to a smaller monochromator with otherwise similar design this has the previously discussed advantages:

(1) The resolution-luminosity product of the instrument becomes larger and

(2) the grating works like a cylindrical grating, so that there is no curvature of the spectral image due to the large horizontal size of the SPEAR source. This will be proved later by raytracing. Therefore, our grating radius will be more than 10 times larger than those considered in previous systems.

Optical analysis and calculated performance

The path function analysis of this monochromator must in principle include the complete optical system, i.e., the condensing mirror M1 and the grating G. Chrisp [19] pointed out that the usual treatment as given by Beutler [13] or Noda et al. [12] using stigmatic divergent rays (eqs. (2)) is not completely correct for the system proposed in the previous section, since the incident wavefront from the entrance slit S1 is astigmatic (convergent in the sagittal and divergent in the meridional plane). Nonetheless we will show that the conventional theory gives a reasonable explanation of the performance of the monochromator as long as only the tangential imaging properties are considered i.e., the spectral resolution. Raytracing of the whole system, later on, provides a check and an accurate evaluation of the performance of the monochromator.

Using equations (2) and (5), we have calculated the individual contributions from the important aberration terms for the scan mode A of the monochromator characterized in

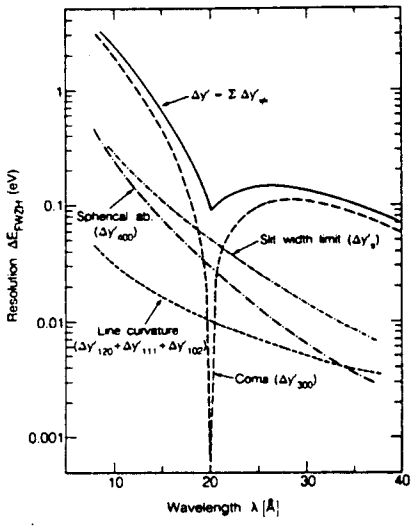

Figure 5. Contributions of various aberrations to the overall energy resolution Δy' of the SGM. Parameters are given in Table 2. Scan mode A (λ_R=20Å).

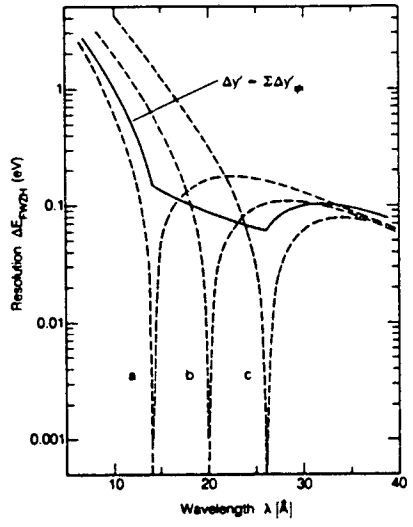

Figure 6. Coma term $\Delta y'_{300}$ for different entrance slit positions. Curves a,b,c correspond to λ_R = 14,20,26Å. The resulting overall resolution is shown as a solid line (mode B/A, see text).

Table 2. These calculations are for an illuminated grating area of 1x15 cm^2. The results are shown in Figure 5 for λ_R = 20Å. Since the exit slit is always adjusted to the best focus, the F_{200} term is zero. At $\lambda = \lambda_R$ the Rowland circle condition is fulfilled, so that the coma term F_{300} becomes zero at this wavelength. For wavelengths which are some Å away from λ_R, coma is obviously the dominant aberration whereas the combined astigmatic coma and line curvature is an order of magnitude smaller. Additionally to the ray aberrations, Figure 5 also includes the slit width limited resolution $\Delta\lambda_S$ given by eq. (1) for a 10μm slit at S1. All calculations are based on the "Full width zero height" (FWZH) criterion. For practical resolutions the "full width half maximum" (FWHM) has to be considered so that the contributions of the aberrations are even somewhat smaller compared to the slit width limit. Therefore, according to Figure 5, it is basically possible to achieve the slit width limited resolution for a 10μm slit as long as the monochromator is operated near λ_R.

Now it is easy to estimate how the system properties are changed when the "Rowland wavelength" λ_R is altered (mode B) or the combined scan mode is used. Figure 6 shows the dominating coma term for three wavelengths λ_R, i.e., the extremes λ_R=14Å (curve a) and λ_R=26Å (curve c), which correspond to the maximum entrance slit movements, and the center λ_R=20Å (curve b) and this figure also shows the resulting overall resolution for the combined scan mode as an enveloping curve. Consequently, the resolution is minimized for output wavelength's λ between 14Å and 26Å and essentially slit width limited. Wavelengths λ ouside this range, which can only be reached with scan mode A, suffer from coma aberration. But even outside this mode B-range the coma contribution can be kept small by choosing λ_R=14 for λ<14Å and λ_R=26 for λ>26Å.

With the raytracing program "Shadow" [21], which was especially designed for synchrotron radiation optics, it is possible to check the above theoretical considerations and to evaluate the overall performance including both optical elements illuminated by a realistic source. The program allowed the use of a realistic gaussian synchrotron source (e.g., σ_x x σ_y = 0.33 x 0.05 cm^2 for λ = 20Å) with a random ray distribution. The total ray output of the source was 5000 of which more than 1200 fell onto M1. The results are shown in Figure 7 for all three gratings. The upper curves 1 show the resolution plots calculated from the raytraces for a slit width of 100μm and keeping this entrance slit in fixed position (mode A, λ_R=20Å). The dashed lines 2 correspond to the same slit positions but 10μm slit width. Optimum resolution which is shown by graphs 3 is obtained with the combined scan mode with $14Å \leq \lambda_R \leq 26Å$ (same as in Figure 6) and 10μm-slits. The curves nicely reproduce the predictions of Figure's 5 and 6. The fact that the resolution is even better than predicted, arises from full width half maximum criterion of Figure 7 compared to the FWZH-calculations of Figures 5 and 6. Also, the illuminated area of the grating might have been slightly different for raytrace and calculation. For an entrance slit width of

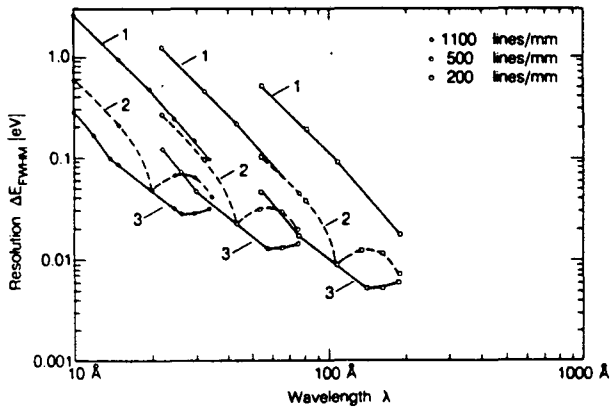

Figure 7. Resolution plots for the SGM (see Table 2) as determnined from ray tracing. Curve 1: fixed entrance slit (100 μm width), Curve 2: fixed entrance slit (10 μm width), Curve 3:· moveable entrance slit (10 μm width).

100 μm (curve 1) the resolution is not much affected by aberrations and is determined mostly by the slit width, so that the performance is approximately the same for modes A and B in this case. If all other resolution limiting factors, e.g. optical surface quality, geometrical stability, etc., are within the required tolerances it should be possible to achieve nearly the very attractive values of Figure 7 (curve 3).

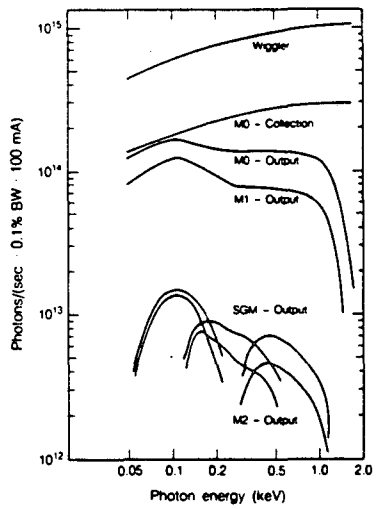

Figure 8. Photon flux at different places along the beamline (M0: plane deflection mirror, M2: refocusing mirror).

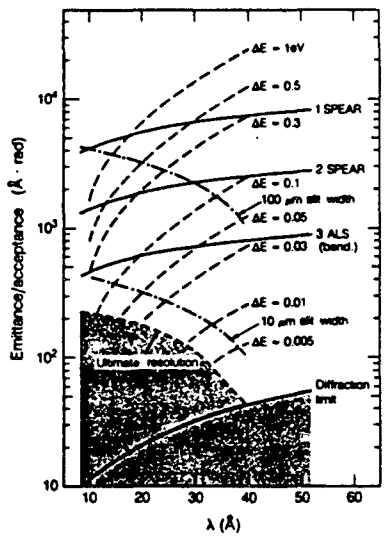

Figure 9. Phase space acceptance of the monochromator compared to the emittance of the source.

Throughput

The power throughput of the beamline was determined with a program which calculates exactly the output of the wiggler source and includes the mirror reflectivities as well as the estimated grating efficiency. Slits were set to yield 0.1% bandwidth. The results, shown in Figure 9 for various places along the conceived SSRL-beamline, promise high output at good resolution and compare favorably with a toroidal grating monochromator since the spherical grating monochromator allows acceptance of the entire horizontal source without introducing aberration.

Since these numbers are specific to the beamline at which the first realization will be installed a better criterion for the light gathering power of this monochromator compared to that of other monochromators and compared to the emittance of the storage ring

is its plot of vertical phase space acceptance against wavelength (see the section on slit width limits). Therefore Figure 9 shows the emittance of the SPEAR ring (as currently used and also with the projected low emittance upgrade) and of a bending magnet on the Berkeley 1-2 GeV synchrotron radiation source (curves 1, 2 and 3 respectively) as well as the phase space acceptance of the monochromator expressed in Å·rad. The long-dashed lines give the acceptance for the case where the monochromator is operated with constant energy resolution ΔE over the whole wavelength range (for the 1100 ℓ/mm-grating) while the dash-dotted curves show the acceptance when the monochromator is operated as usual, with the entrance slit kept at a fixed width (slit width limit, grating fully illuminated). Comparison of all these sets of curves yields information about how much of the incoming flux is necessarily lost by overfilling either the spatial or angular aperture of the instrument at a desired resolution. The ultimate theoretical resolution is limited by spherical aberration (short dashed line) and diffraction as shown by the shaded area.

Acknowledgements

The authors wish to acknowledge helpful conversations on this work with M. Hettrick, J. Underwood and F. Cerrina. This work was supported by the Office of Basic Energy Sciences, U.S. Department of Energy, under Contract # DE-AC03-76SF00098.

REFERENCES

1. R.L. Johnson, Handbook on Synchrotron Radiation, ed. E.E. Koch, North Holland Amsterdam, Vol. 1A, chapter III, 1983.
2. H. Petersen, Nucl. Instr. and Meth. A246, 260 (1986).
3. F.J. Himpsel et al., Nucl. Instr. and Meth. 222, 107 (1984).
4. W. Eberhardt, private communication
5. R. Giacconi et al., Astrophys. J. 230, (1979).
6. D.A. Schwartz et al., Proc. SPIE 597, 10 (1985).
7. e.g., the WYKO Optical Profiler with 2.5x Objective (5mm trace length) and the Zygo Mark III interferometer.
8. P. Glenn and A. Slomba, Proc. SPIE 597, 55 (1985).
9. K. Ito, T. Namioka, Y. Morioka, T. Sasaki, H. Noda, K. Goto, T. Katayama and M. Koike, Appl. Opt. 25, 837 (1986).
10. Milton Roy, replica grating #35-52-77-710, made from a master grating ruled 30 years ago on a substrate made at the now defunct Bausch & Lomb optical shop. The figure was tested by the Foucault test.
11. G. Hertzberg, Proc. Roy. Soc. A234, 516 (1956).
12. H. Noda, T. Namioka and M. Seya, J. Opt. Soc. Am 64, 1031 (1974).
13. H.G. Beutler, J. Opt. Soc. Am. 35, 311 (1945).
14. W.T. Welford, in Progress in Optics, Vol. 4, chapter VI, North Holland, Amsterdam, 1965.
15. J.E. Mack, J.R. Stehn, and B. Edlén, J. Opt. Soc. Am. 22, 245 (1932).
16. "1-2 GeV Synchrotron Radiation Source", Conceptual design report, Pub-5172 Rev., Lawrence Berkeley Laboratory, 1986.
17. W.A. Rense, T. Violett, J. Opt. Soc. Am 49, 139 (1959).
18. G. Tondello, Optica Acta 26, 357 (1979), A.M. Malvezzi, L. Garifo, G. Tondello, Appl. Opt. 20, 2560 (1981).
19. M.P. Chrisp, Appl. Opt. 22, 1519 (1983).
20. M.C. Hettrick and J.H. Underwood, Appl. Opt. 25, 4228 (1986).
21. B. Lai, F. Cerrina, Nucl. Instr. and Meth. A246, 337 (1986).

This report was done with support from the Department of Energy. Any conclusions or opinions expressed in this report represent solely those of the author(s) and not necessarily those of The Regents of the University of California, the Lawrence Berkeley Laboratory or the Department of Energy.

Reference to a company or product name does not imply approval or recommendation of the product by the University of California or the U.S. Department of Energy to the exclusion of others that may be suitable.

LAWRENCE BERKELEY LABORATORY
TECHNICAL INFORMATION DEPARTMENT
UNIVERSITY OF CALIFORNIA
BERKELEY, CALIFORNIA 94720